Clay Minerals, (2018) **53**, 525–544

Adsorption capacity of sodic- and dendrimers-modified stevensite

MOHAMED HAJJAJI[1,*], ABDELLAH BERAA[1,2,3], YANNICK COPPEL[2,3], RÉGIS LAURENT[2,3] AND ANNE-MARIE CAMINADE[2,3]

[1] *Laboratoire de Physico-chimie des Matériaux et Environnement, Unité Associée au CNRST (URAC 20), Faculté des Sciences Semlalia, Université Cadi Ayyad, B.P. 2390, Av. Pce My Abdellah, 40001, Marrakech, Morocco*

[2] *CNRS, LCC (Laboratoire de Chimie de Coordination du CNRS), 205 route de Narbonne, BP 44099, F-31077 Toulouse Cedex 4, France*

[3] *Université de Toulouse, UPS, INPT, F-31077 Toulouse Cedex 4, France*

(*Received 13 March 2017; revised 3 June 2018; Associate Editor: Laurent Michot*)

ABSTRACT: The adsorption capacities of nano-sized organoclays composed of a stevensite-rich clay (R), phosphorus dendrimers (GC1 and GC2) and Na^+-saturated clay were evaluated for their capacity to adsorb chromate and methylene blue (MB) in the range of 298–318 K. The adsorption kinetics and the isotherms were analysed based on kinetic equations and isotherm models and by adopting a non-linear regression procedure. In addition, the organoclays and the Na^+-saturated clays were characterized principally by solid-state nuclear magnetic resonance spectroscopy. The pseudo-second-order rate equation described kinetics data well, and the adsorption rates were not limited by the intraparticle diffusion or by the liquid film diffusion. Both chemical species were adsorbed spontaneously ($-31 < \Delta G°_T < -10$ kJ/mol), but the adsorbents had a high affinity for MB species. The adsorption isotherms of chromate were fitted better by the Freundlich model, while those of MB followed the Langmuir model. Chromate adsorption took place at the edges and the free surfaces of stevensite, particularly at the protonated aluminols. MB was adsorbed as MBH^{2+} and MB^+. The MB protonation occurred at the clay surfaces, and MB^+ ions were located at the planar surfaces of stevensite as well as at the external surfaces of aggregates. Moreover, the tetrahedral sheet of stevensite involved in the formation of GC1-based organoclays was the subject of a partial chemical modification.

KEYWORDS: stevensite, dendrimers, chromate, methylene blue, adsorption, characterization.

To increase the adsorption capacity and reduce the treatment time of contaminated water, nano-sized adsorbents have been designed. Clay minerals, especially those belonging to the smectite group, are suitable materials for the design of nanoadsorbents. The use of smectites was justified by their nanostructure and relatively large specific surface area and cation exchange capacity (CEC), as well as their ability to accept chemical species in the interlayer space. Stevensite is a trioctahedral smectite that might interact spontaneously with cationic chemical pollutants (heavy metals, basic dyes) and some polarized organic molecules. However, because of its negative charge, due to vacancies in the octahedral sheet, the adsorption of anionic chemical species such as chromate is very limited (Ren *et al.*, 2014; Shokri *et al.*, 2017). To overcome such limitations and enhance the uptake of various chemical pollutants, smectite (*e.g.* montmorillonite) has been the subject of various modifications (acid or alkaline etching, intercalation, *etc.*) (Heinz, 2012; Lee & Tiwari, 2012; Mache *et al.* 2015; Chang *et al.*, 2016; Krupskaya *et al.*, 2017).

*E-mail: hajjaji@uca.ma
https://doi.org/10.1180/clm.2018.39

Hexavalent chromium (Cr^{VI}) is a powerful oxidant and is highly toxic to human beings (Saha *et al.*, 2011; Zhitkovich, 2011). Cr^{VI} is encountered in effluents of leather tanning, dyeing and electroplating, among others. It is mostly present in the form of anions (CrO_4^{2-}, $Cr_2O_7^{2-}$, $HCrO_4^-$), which are highly mobile species in aqueous solutions and might easily enter groundwater (Zhitkovich, 2011). To comply with the international recommendations (WHO, 2003), Cr^{VI}-containing effluents must be remediated. The permissible amount of total chromium in drinking water is <0.05 mg/L (WHO, 2003).

Removal of Cr^{VI} might be achieved by adsorption, which has proven to be an efficient and popular remediation process (*e.g.* Fu & Wang, 2011). Activated carbon is a versatile adsorbent, but in order to find suitable local alternatives, many adsorption studies have been undertaken on natural or modified geomaterials including clays (Akar *et al.*, 2009; Ajouyed *et al.*, 2010; Santhana *et al.*, 2012; Setshedi *et al.*, 2013; Zhao *et al.*, 2013; Hajjaji & Beraa, 2015; Rathnayake *et al.*, 2017). However, little attention has been paid to the use of nanocomposites of clays and dendrimers.

Methylene blue is an organic cationic colorant used in the dyeing of textiles. MB-rich effluents have adverse effects on fauna and flora (Sarkar *et al.*, 2010). The harmful effects of MB on human beings manifest themselves as the dose exceeds 2 mg/kg. The removal of MB from aqueous solutions by clay minerals, particularly those belonging to the smectite group, has been studied extensively (Cottet *et al.*, 2014; Ranđelović *et al.*, 2014; Chang *et al.*, 2016; Chakraborty *et al.*, 2017). However, few investigations have been carried out on the adsorption of MB by stevensite (Bouna *et al.*, 2010).

Phosphorus-based dendrimers are synthesized macromolecules with a spherical shape and branches emanating radially from a central core (Caminade & Majoral, 2016). They are nano-sized materials and can have peripheral cationic groups such as ammonium groups (Padié *et al.*, 2009) that may be attached spontaneously to clay mineral particles. Hence, new hybrid materials with specific adsorptive properties can be formed.

This work is complementary to our studies related to the adsorption abilities of phosphorus dendrimers-containing organoclays (Beraa *et al.*, 2016, 2017). In this study, the kinetics and the equilibrium processes of the adsorption of chromate and MB on organoclays of stevensite-rich clays and phosphorus dendrimers and on Na^+-saturated clays are investigated at varying temperature gradients. In addition, the adsorption mechanisms are discussed in relation to the results of the structural characterization of stevensite.

MATERIALS

Dendrimers

The first and second generations (GC1 and GC2, respectively) of phosphorus-based dendrimers were synthesized by a divergent method following the reaction paths illustrated in Fig. 1. Details of the experimental protocol were given by Caminade & Majoral (2016). To obtain water-soluble and positively charged dendrimers, the terminal groups of the dendrimers were substituted with ammonium groups using N,N-diethylethylenediamine as a reactant. The cationic dendrimers obtained were freeze-dried and stored in a drying oven at 80°C.

The hydrodynamic radii (R_H) of GC1 and GC2 were 1.1 and 1.5 nm, respectively. Details of the determination of R_H are given below.

Clay characterization

The clay, referred to hereafter as R, was a commercial Fuller's earth used in traditional cosmetics preparations. It originates from Jbel Rhassoul (Morocco).

According to the clay characterization results reported by Christidis & Koutsopoulou (2013) and based on the X-ray diffraction (XRD) trace (Fig. 2), the clay is composed of stevensite and non-clay minerals, mainly dolomite. The amount of stevensite estimated by the reference intensity ratio (RIR) method using the *X'Pert HighScore* software (*e.g.* Degen *et al.*, 2014) is 72%.

The presence of the main minerals identified was confirmed by the Fourier-transfrom infrared (FTIR) spectrum (Fig. 3).

The chemical composition of the clay given in Table 1 confirmed the magnesian character of the clay mineral identified, the presence of carbonate and possible substitution of Mg^{2+} by Al^{3+} in the octahedral sheet.

The BET specific surface area and the CEC (Table 1) corresponded well with those of smectite clay materials, and they were in line with those reported for stevensite-rich clay (*e.g.* Elass *et al.*, 2011).

Referring to the International Union of Pure and Applied Chemistry (IUPAC) classification of adsorption isotherms (Al Othman, 2012), the N_2 adsorption/desorption isotherm of the clay (Fig. 4a) is type H4. Accordingly, the clay is considered a mesoporous material (Al Othman, 2012).

https://doi.org/10.1180/clm.2018.39 Published online by Cambridge University Press

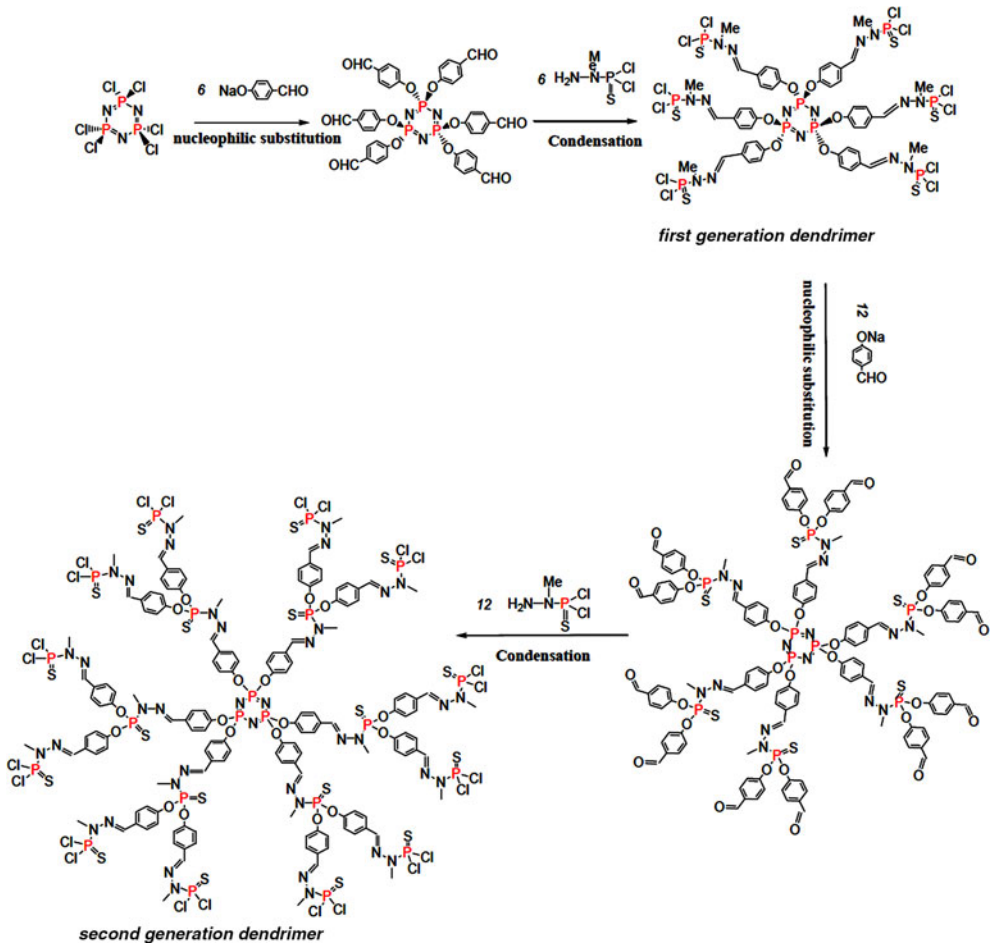

FIG. 1. Schematic representation of the reaction paths of the synthesis of the first- and second-generation dendrimers (GC1 and GC2).

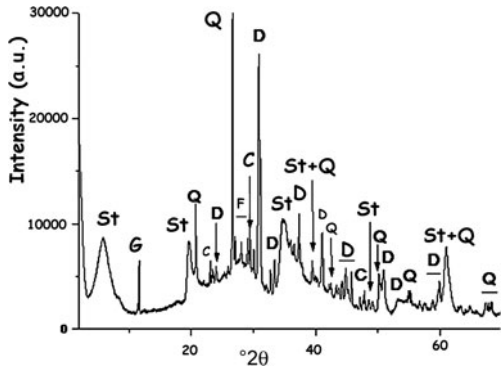

FIG. 2. XRD trace of the clay used (R). St = stevensite; G = gypsum; Q = quartz; C = calcite; F = K-feldspar; D = dolomite.

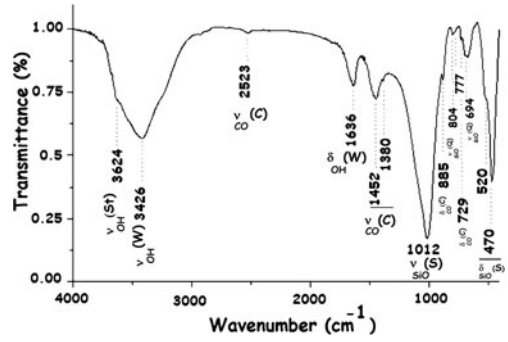

FIG. 3. FTIR spectrum of the R clay. St = stevensite; W = water; C = carbonates (dolomite/calcite); S = silicate; Q = quartz.

https://doi.org/10.1180/clm.2018.39 Published online by Cambridge University Press

TABLE 1. Chemical composition and some physical properties of the clay used.

Chemical composition (mass %)								
SiO_2	Al_2O_3	MgO	Fe_2O_3	Na_2O	CaO	K_2O	TiO_2	SO_3
49.9	5.5	31.8	0.9	0.7	7.0	0.8	0.1	2.4
BET (m^2/g)					CEC (meq/g)			
132							0.73	

BET = Brunauer–Emmett–Teller specific surface area; CEC = cation exchange capacity.

Adsorbates

The MB used ($C_{16}H_{18}N_3SCl$; MW: 319.86 g/mol, Merck) was of 95% purity. Potassium chromate (K_2CrO_4, Fisher Scientific) with >99% purity was the source of Cr^{VI}.

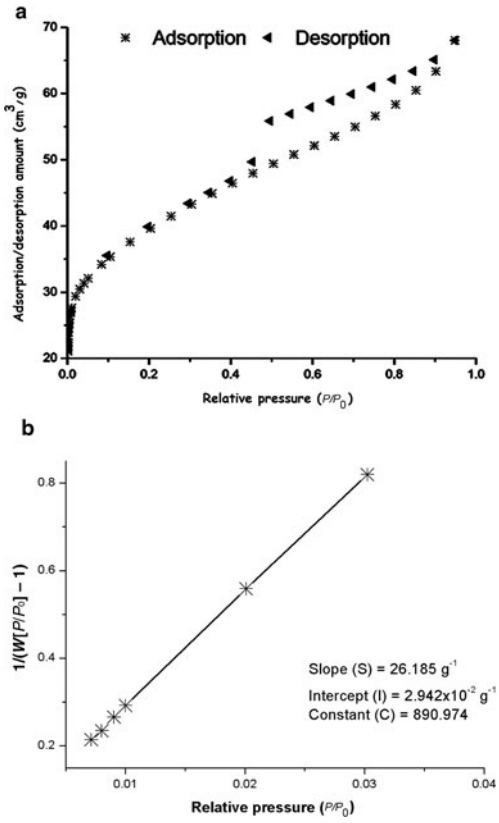

FIG. 4. N_2 adsorption/desorption isotherms of the clay (a) and plot of $1/(W[P/P_o] - 1)$ *vs.* relative pressure (b).

METHODS

Preparation of nanocomposites

A total of 0.5 g of dried cationic dendrimers (GC1 or GC2) was dissolved in 20 mL of warm water (353 K). The solution of the dendrimers obtained was mixed with 10 mL of a dispersion of Na^+-saturated clay (3.5 g). The mixture with pH = 6.3 (natural pH) was stirred for 24 h at room temperature, and the solid fraction was separated by centrifugation and freeze-dried.

Referring to our previous study related to the characterization of the nanocomposites prepared (Beraa *et al.*, 2017), these organoclays were composed of intercalated and exfoliated nanocomposites. The relative abundance of these nanocomposites depended on the size of the dendrimers.

Preparation of sodium-saturated clay

Portions (40 g) of the <80 μm fraction of R were added to NaCl aqueous solutions (0.5 M) and shaken for 24 h. The Na^+-saturated clay was isolated by centrifugation (4000 rpm) and washed with distilled water until the rinse water was free of Cl^- ions ($AgNO_3$ test).

Kinetic experiments

The kinetic experiments of the adsorption of chromate on Na^+-R, GC1-R or GC2-R were carried out on mixtures composed of 40 mL of a solution of K_2CrO_4 (0.04 mmol/L) and 16 mL of the dispersion (0.5 g/L) of the tested adsorbent. For the experiments involving MB, 40 mL of a solution of MB (0.04 mmol/L) were mixed with 16 mL of the dispersion of the enumerated adsorbents. The temperature of the mixture was kept constant at 298, 308 or 318 K. The pH of the mixture was adjusted to 4 by adding a few droplets of 0.1 M solution of HCl or NaOH. At

https://doi.org/10.1180/clm.2018.39 Published online by Cambridge University Press

this pH, the amounts of chromate and MB retained were relatively significant. The mixtures prepared were stirred with a laboratory magnetic stirrer at 250 rpm. Samples of the mixtures were taken out at regular times and were centrifuged immediately (4000 rpm) for <3 min. The amount of chromate in the isolated supernatant (C_t; mmol/L) was determined with UV-visible spectrometry according to the experimental method described by Soares *et al.* (2009). The quantity of chromate retained (q_t; mmol/g) was deduced from equation 1:

$$q_t = \frac{(C_o - C_t)V}{m} \quad (1)$$

where C_o (mmol/L) is the initial concentration of chromate, V is the volume of solution (L) and m is the weight of adsorbent (g).

The amount of MB retained was also determined according to equation 1. For this purpose, the amount of MB in the supernatant (C_t) was measured at 664 nm with a UV-visible spectrophotometer, JP Selecta. For both studies, the experiments were run in duplicate.

Because of the shortcoming of using the linearized forms of the kinetic equations (*e.g.* Hossain *et al.*, 2013), the experimental kinetic data were analysed with the non-linear forms of the pseudo-first-order (equation 2) and the pseudo-second-order (equation 3) kinetic equations:

$$q_t = q_e\ (1 - e^{-k_1 t}) \quad (2)$$

$$q_t = \frac{k_2 q_e^2 t}{1 + k_2 q_e t} \quad (3)$$

where k_1 and k_2 are the pseudo-first-order and the pseudo-second-order rate constants, respectively, and q_e is the uptake quantity of the adsorbate at equilibrium.

The non-linear regression analysis was performed using the solver add-in of *Microsoft Excel*™ (Hossain *et al.*, 2013). The best fit of the experimental and theoretical curves was reached with a trial-and-error procedure and was supported by the coefficient of determination (R^2) according to equation 4:

$$R^2 = 1 - \frac{\sum (q_t - q_t^c)^2}{\sum (q_t - q_t^a)^2} \quad (4)$$

where q_t and q_t^c are the experimental and calculated instantaneously retained quantities of adsorbate and q_t^a is the average of the values of q_t.

The experimental values were also compared to the calculated ones by using the normalized standard deviation (NSD) (Hossain *et al.*, 2013):

$$NSD = 100\sqrt{\frac{1}{n-1}\sum_1^n \left[\frac{q_t - q_t^c}{q_t}\right]^2} \quad (5)$$

where n is the number of experimental runs. The best fit is indicated by the smaller value of NSD.

Batch adsorption equilibrium

For the plot of the equilibrium isotherms, aqueous mixtures composed of 40 mL of a solution of chromate or MB (10^{-3}–8×10^{-2} mmol/L), 16 mL of a solution (0.5 g/L) of Na^+-R, GC1-R or GC2-R and 24 mL of distilled water were maintained at constant temperatures (298, 308 or 318 K) for 4 h. The mixtures were stirred (250 rpm) at constant pH 4. The amounts of chromate and MB retained at equilibrium (q_e; mmol/g) were measured as reported previously.

Because of the limitations of using the linear forms of the equations of the adsorption isotherms (Hossain *et al.*, 2013), the isotherms of the adsorption of chromate and MB on the studied sorbents were fitted to the non-linear forms of the Langmuir model (equation 6; Langmuir, 1918), the Freundlich model (equation 7; Freundlich, 1907) and the Harkins–Jura model (equation 8; Harkins & Jura, 1943).

$$q_e = \frac{K_L q_e^{max} C_e}{1 + K_L C_e} \quad (6)$$

$$q_e = K_F C_e^{1/n} \quad (7)$$

$$q_e = \left(\frac{B'}{A} - \frac{log C_e}{A}\right)^{-1/2} \quad (8)$$

where q_e is the uptake amount at equilibrium, K_L is the Langmuir constant, q_e^{max} is the adsorption capacity, K_F is the Freundlich constant and n, A and B' are constants.

These models were selected because of the different hypotheses about the adsorption mechanisms that are discussed below. The fitting of the models to the experimental isotherms was accomplished by the solver add-in of *Microsoft Excel*™. The degree of closeness of the experimental data to the predicted outcomes was also evaluated by calculating the residual root mean square error (RMSE) (Hossain *et al.*, 2013) (equation 9):

$$RMSE = \sqrt{\frac{1}{n-1}\sum_1^n (q_e^{exp} - q_e^{cal})^2} \quad (9)$$

https://doi.org/10.1180/clm.2018.39 Published online by Cambridge University Press

where q_e^{exp} and q_e^{cal} are the experimental and the predicted uptake amounts at equilibrium. The best fit corresponds to the smaller value of RMSE.

Methods and investigation techniques

The hydronamic radius, R_H, was calculated from the formula in equation 10 (*e.g.* Hameau *et al.*, 2015):

$$R_H = \frac{k_B T}{6\pi\eta_s D} \quad (10)$$

where k_B is Boltzmann's constant ($1.38064852 \times 10^{-23}$ J K^{-1}), T is the operating temperature (298 K), η_s is viscosity of the medium (tetrahydrofuran; $\eta_s = 4.8 \times 10^{-4}$ Pa s^{-1}) and D is the diffusion coefficient (m^2 s^{-1}). For measurement of D, a NanoDLS particle size analyser (Brookhaven Instruments, Holtsville, NY, USA) was used. The apparatus was calibrated using 92 ± 4 nm NanoLatex, and the laser beam intensity was optimized automatically. The scattering angle was 90°, and the results were analysed with the method of cumulant (Mailer *et al.*, 2015).

The CEC of the clay was measured using cobaltihexamine as an index cation (Aran *et al.*, 2008). The uptake amount of cobaltihexamine was evaluated from the Beer–Lambert law using a UV-visible spectrophotometer, JP Selecta (λ = 476 nm) .

The BET specific surface area (A_s) was calculated according to the equations 11 and 12:

$$A_s = \frac{W.N.A_c}{M} \quad (11)$$

$$W = \frac{1}{(S+I)} \quad (12)$$

where S and I were determined from the plot of Fig. 4b by means of a Quantachrome Autosorb-iQ apparatus, using nitrogen as the adsorbate. N is Avogadro's number (6.022×10^{23}/mol), A_c is the cross-section area of N_2 (16.2×10^{-2} nm^2/molecule) and M = 28.013 g/mol.

The X-ray diffraction (XRD) analysis of the adsorbents before and after contact with chromate and MB was performed with an X'Pert-PRO diffractometer operating with a copper anode ($K\alpha$ = 1.5418 Å) under the following conditions: 40 mA, 45 kV; step scanning: 0.017°; scan step time: 400.05 s. The chemical composition of the clay was determined with an S4 Pioneer X-ray fluorescence (XRF) spectrometer (excitation: end window Rh X-ray tube, 75 µm Be window, 2.7 kW, 60 kV maximum, 100 mA maximum) on pressed powder samples in argon (90%) and methane (10%) atmosphere. The Fourier-transform infrared spectrum of the clay was recorded in the range of 4000 to 400 cm^{-1} with a Perkin Elmer 1725 spectrophotometer at 4 cm^{-1} resolution, on KBr disks (1:100 clay:KBr ratio). Solid-state nuclear magnetic resonance (NMR) spectra were recorded at ambient temperature on a Bruker Avance III 400WB apparatus. The frequencies used were 8 kHz for ^{1}H, ^{23}Na and ^{29}Si and 9 kHz for ^{27}Al. The recycle delays were 5, 2, 3 and 30 s for ^{1}H, ^{23}Na, ^{27}Al and ^{29}Si, respectively. For ^{23}Na analysis, a solution of NaCl (1 M) was used as the reference. The tetramethylsilane was used as the reference for ^{1}H and ^{29}Si. The reference for ^{27}Al analysis was a diluted aqueous solution of NaCl containing $Al(H_2O)_6^{3+}$.

RESULTS AND DISCUSSION

Kinetic study

The kinetics of the adsorption of MB and chromate species on both organoclays (GC1-R, GC2-R) and Na^+-saturated clays was fast in the investigated range of temperatures, and saturation was reached in <30 min (Figs 5, 6).

The non-linear regression analysis of the kinetic data indicated that the experimental curves followed the pseudo-second-order kinetics equation (Table 2). This result suggested that the adsorption rates of both chemical species were mainly controlled by the interaction between the active sites of adsorbent and adsorbate species. The rate constants of the adsorption of chromate on GC2-R were relatively high (Table 2), probably due to its specific structural characteristics and/or its particular interactions with chromate species discussed below.

The variation of the rate constant (k_2) *vs.* the reciprocal temperature indicated that the Arrhenius equation:

$$k_2 = Ae^{-\frac{E_a}{RT}} \quad (13)$$

where A is the frequency factor, E_a is the activation energy (J/mol) and R is the gas constant (8.314 J K^{-1} mol^{-1}) was followed only for the adsorption of MB and chromate on GC1-R. The calculated values of E_a were 6.070 and 1.171 kJ/mol for MB and chromate, respectively.

The rate-limiting steps were evaluated using the intraparticle diffusion model (Ismadji *et al.*, 2015):

$$q_t = k_i t^{0.5} \quad (14)$$

https://doi.org/10.1180/clm.2018.39 Published online by Cambridge University Press

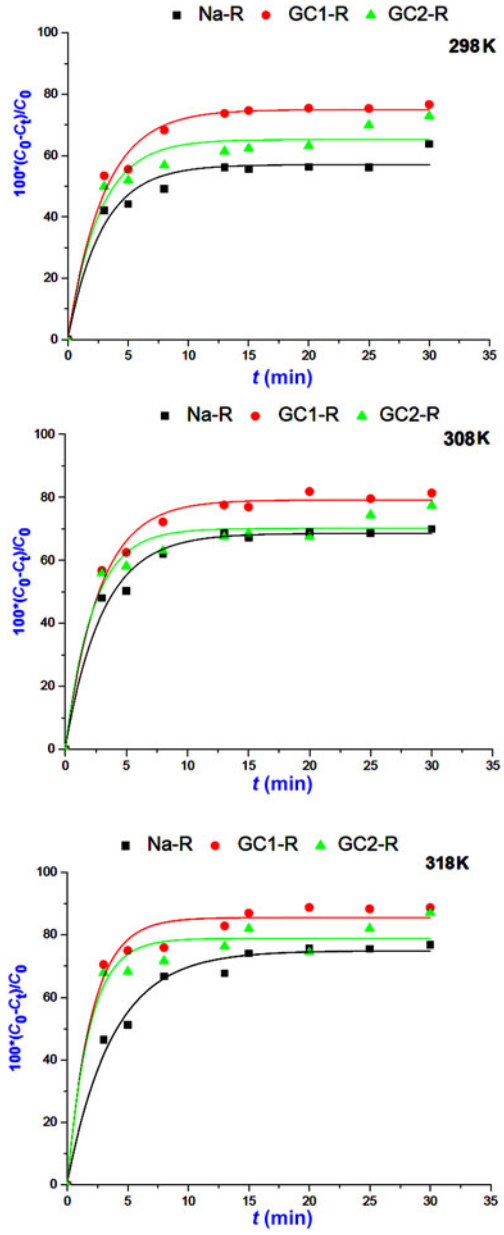

FIG. 5. Kinetics curves of the adsorption of methylene blue on Na^+-R, GC1-R and GC2-R.

where k_i is the intraparticle diffusion coefficient (mmol/g $min^{0.5}$), and the liquid film diffusion model (Qiu *et al.*, 2009):

$$\mathrm{Ln}\frac{C_t}{C_o} = -k_{ld}t \qquad (15)$$

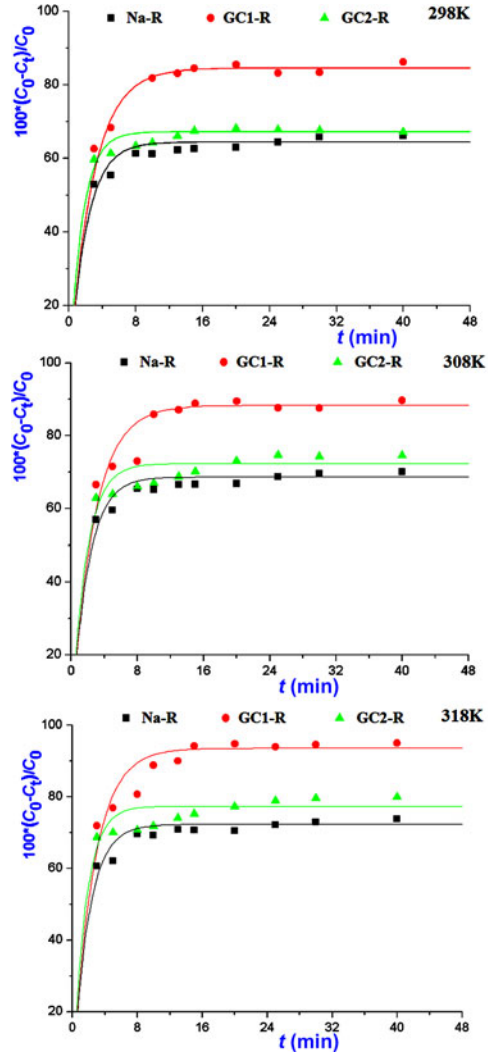

FIG. 6. Variations in the amounts of chromate retained instantaneously by the absorbents studied.

where $k_{ld} = k_f\ (S/V)$, k_f is the external diffusion coefficient (cm/min), S is the external surface area of the adsorbent and V is the volume of the solution.

The values of k_i and k_{ld} and the constants C and C' (Table 3) were deduced from the slopes and the intercepts of the plots of $q_t = f(t^{0.5})$ and $\mathrm{Ln}(C_t/C_o) = f(t)$ (not shown). C and C' are indicative of the thickness of the boundary layer of the adsorbates built up around adsorbent particles. The absence of such a boundary is expressed by C (or C') = 0. Based on the fact that C and C' were different from zero, and taking into consideration

https://doi.org/10.1180/clm.2018.39 Published online by Cambridge University Press

TABLE 2. Parameters and non-linear regression coefficients (coefficient of determination [R^2], normalized standard deviation [NSD]) related to the pseudo-first-order (PFKE) and pseudo-second-order (PSKE) kinetics equations.

Adsorbent	Model	Parameter	Temperature (K)			q_e^{exp} (mmol/g)		
			298	308	318	298 K	308 K	318 K
MB								
Na-R	PFKE	k_1 (s^{-1})	0.004	0.005	0.004	0.17	0.19	0.22
		q_e^{cal} (mmol/g)	0.17	0.19	0.22			
		R^2	0.673	0.907	0.890			
		NSD	9.079	4.279	5.853			
	PSKE	k_2 (mmol g^{-1} s^{-1})	0.040	0.053	0.027			
		q_e^{cal} (mmol/g)	0.19	0.20	0.24			
		R^2	0.895	0.901	0.955			
		NSD	4.987	3.831	3.672			
GC1-R	PFKE	k_1 (s^{-1})	0.005	0.005	0.007	0.21	0.22	0.25
		q_e^{cal} (mmol/g)	0.21	0.22	0.25			
		R^2	0.860	0.812	0.582			
		NSD	5.002	5.182	6.210			
	PSKE	k_2 (mmol g^{-1} s^{-1})	0.043	0.046	0.050			
		q_e^{cal} (mmol/g)	0.23	0.24	0.26			
		R^2	0.936	0.923	0.907			
		NSD	3.339	2.996	2.999			
GC2-R	PFKE	k_1 (s^{-1})	0.004	0.005	0.007	0.20	0.21	0.25
		q_e^{cal} (mmol/g)	0.20	0.21	0.25			
		R^2	0.538	0.497	0.583			
		NSD	10.990	10.241	8.747			
	PSKE	k_2 (mmol g^{-1} s^{-1})	0.033	0.035	0.029			
		q_e^{cal} (mmol/g)	0.21	0.23	0.27			
		R^2	0.814	0.829	0.688			
		NSD	7.041	6.189	6.178			

(continued)

TABLE 2. (*contd.*)

Adsorbent	Model	Parameter	Temperature (K)			q_e^{exp} (mmol/g)		
			298	308	318	298 K	308 K	318 K
Chromate								
Na-R	PFKE	k_1 (s^{-1})	0.008	0.008	0.009	0.18	0.19	0.20
		q_e^{cal} (mmol/g)	0.18	0.19	0.20			
		R^2	0.858	0.846	0.836			
		NSD	3.789	3.850	3.903			
	PSKE	k_2 (mmol g^{-1} s^{-1})	0.099	0.096	0.099			
		q_e^{cal} (mmol/g)	0.19	0.20	0.21			
		R^2	0.975	0.971	0.964			
		NSD	1.578	1.649	1.843			
GC1-R	PFKE	k_1 (s^{-1})	0.006	0.006	0.007	0.24	0.25	0.26
		q_e^{cal} (mmol/g)	0.24	0.25	0.26			
		R^2	0.850	0.845	0.861			
		NSD	5.481	5.406	4.677			
	PSKE	k_2 (mmol g^{-1} s^{-1})	0.049	0.050	0.051			
		q_e^{cal} (mmol/g)	0.25	0.26	0.27			
		R^2	0.928	0.919	0.957			
		NSD	3.531	3.602	2.446			
GC2-R	PFKE	k_1 (s^{-1})	0.011	0.010	0.011	0.19	0.20	0.22
		q_e^{cal} (mmol/g)	0.19	0.20	0.22			
		R^2	0.867	0.744	0.740			
		NSD	3.110	4.964	4.754			
	PSKE	k_2 (mmol g^{-1} s^{-1})	0.156	0.100	0.107			
		q_e^{cal} (mmol/g)	0.19	0.21	0.22			
		R^2	0.969	0.930	0.921			
		NSD	1.470	2.639	2.673			

MB = methylene blue.

TABLE 3. Parameters of the intraparticle diffusion and the liquid film diffusion models calculated for different temperatures, and the fitting coefficients of the models.

Adsorbate			Chromate			MB		
Model	Adsorbent	Parameters	298 K	308 K	318 K	298 K	308 K	318 K
Intraparticle diffusion	Na^+-R	k_i (mmol/g $min^{0.5}$)	0.01	0.01	0.01	0.02	0.02	0.03
		R^2	0.795	0.777	0.728	0.879	0.813	0.830
		C (mmol/g)	0.13	0.15	0.15	0.09	0.10	0.08
	GC1-R	k_i (mmol/g $min^{0.5}$)	0.03	0.03	0.03	0.03	0.03	0.02
		R^2	0.856	0.853	0.933	0.825	0.920	0.948
		C (mmol/g)	0.13	0.14	0.16	0.11	0.12	0.16
	GC2- R	k_i (mmol/g $min^{0.5}$)	0.01	0.01	0.01	0.01	0.01	0.01
		R^2	0.979	0.974	0.953	0.848	0.791	0.486
		C (mmol/g)	0.15	0.16	0.17	0.11	0.13	0.17
Liquid film diffusion	Na^+-R	K_{ld} (min^{-1})	0.02	0.02	0.03	0.02	0.03	0.05
		R^2	0.797	0.803	0.786	0.801	0.733	0.786
		C’	−0.73	−0.73	−0.86	0.53	0.64	0.59
	GC1-R	K_{ld} (min^{-1})	0.08	0.10	0.13	0.04	0.05	0.06
		R^2	0.879	0.883	0.935	0.764	0.914	0.949
		C’	−0.74	−0.76	−1.29	0.73	0.70	1.05
	GC2-R	K_{ld} (min^{-1})	0.02	0.02	0.02	0.02	0.02	0.02
		R^2	0.996	0.996	0.959	0.835	0.746	0.379
		C’	−0.86	−0.93	−1.09	0.64	0.78	1.06

MB = methylene blue.

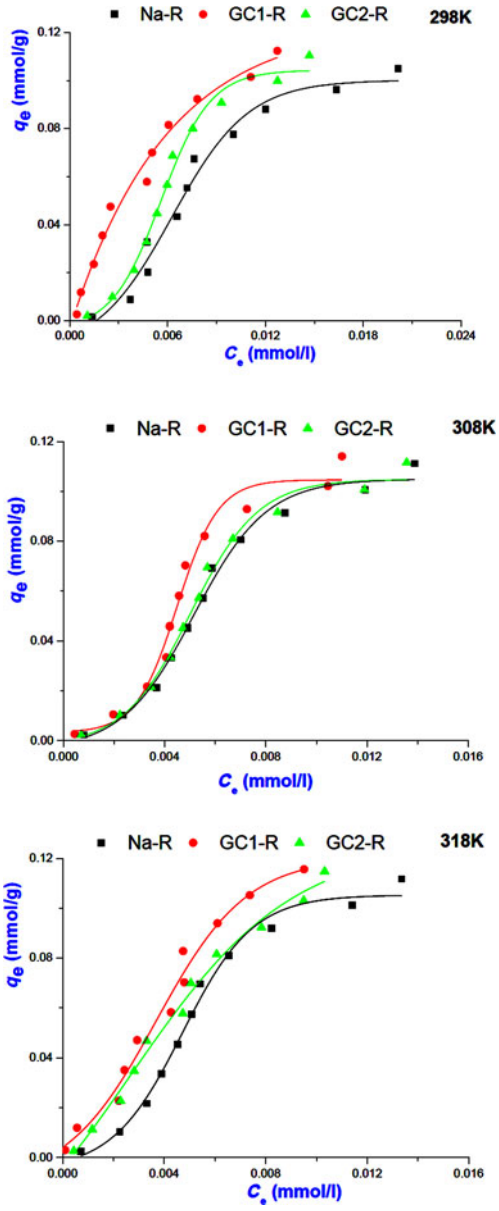

FIG. 7. Isotherms of MB adsorption on Na^+-R, GC1-R and GC2-R.

the values of the fitting coefficient (Table 3), the adsorption processes of chromate and MB were not controlled by diffusion within particles or by diffusion through the liquid film around adsorbent particles. These results supported the above hypothesis, namely that the rates of the adsorption processes were mainly controlled by chemisorption.

Equilibrium studies

The analysis of the experimental adsorption isotherms of MB (Fig. 7) using the non-linear forms of the above models (equations 6 and 7) indicated that the isotherms of Na-R and GC2-R and that of GC1-R plotted at 298 K were fitted better by the Langmuir model (Table 4). Hence, MB adsorption probably occurred on identical active sites, and no more than a monolayer of MB species was built around adsorbent particles at saturation. Probably because of this fact, the maximum uptake amounts of MB (Table 4) were less than or close to the CEC of the clay (0.73 meq/g).

Considering the calculated values of the Gibbs free energy ($\Delta G°_T = -RT\text{LnK}$, where R is the gas constant and K is the equilibrium constant taken here as the Langmuir constant K_L) (Table 5), MB adsorption occurred spontaneously. Based on the algebraic values of heat ($\Delta H°_T$) and entropy ($\Delta S°_T$) (Table 5), the adsorption of MB on Na-R and GC2-R was exothermic and occurred because of an increase of the dispersal of energy, probably the energy of the bonds between MB species and the active sites of the adsorbents.

The isotherms of the adsorption of MB on GC1-R at 308 and 318 K were described better by the Freundlich model, and the parameter 1/n was slightly less than unity (Table 4). These results suggested that MB adsorption at these temperatures was less favoured and took place on heterogeneous sites. The analysis of the equilibrium data using the non-linear form of the model of Harkins–Jura (equation 8) did not lead to reasonable R^2 values. Thus, the involvement of the eventual active pore sites of adsorbents in MB adsorption was rejected.

Regarding the adsorption isotherms of chromate (Fig. 8), the non-linear regression analysis of the equilibrium data showed that the isotherms were described reasonably well by the Freundlich model (Table 4) and adsorption was more favourable ($1/n > 1$). Similar to the MB isotherms, the model of Harkins–Jura was not successful, and consequently the contribution of the sites of pores to the adsorption of chromate was discarded.

The equilibrium constant, K_e, of the adsorption of chromate on the absorbents studied was identified as the intercept of the linear curve of $q_e/C_e = f(q_e)$ ($q_e \to 0$ for very dilute solution) and was used for the calculation of the Gibbs free energy (Table 5).

Adsorption of chromate on the absorbents studied took place spontaneously, and the adsorption was endothermic for Na-R and GC1-R. Moreover, $\Delta H°$ and $\Delta S°$ associated with the adsorption of chromate on

https://doi.org/10.1180/clm.2018.39 Published online by Cambridge University Press

TABLE 4. Values of the parameters and non-linear regression coefficients (coefficient of determination [R^2], root mean square error [RMSE]) related to the adsorption isotherms adopted.

Adsorbent	Model	Parameters	Temperature (K)		
			298	308	318
MB					
Na-R	Langmuir	K_L (L/mol)	23,653	20,000	20,500
		q_e^{max} (mmol/g)	0.35	0.54	0.56
		R^2	0.904	0.920	0.918
		RMSE	0.0110	0.0105	0.0107
	Freundlich	K_F ($[10^{-3}mol^{(1-1/n)}L^{1/n}]/g$)	2693	2700	2000
		1/n	0.922	0.896	0.865
		R^2	0.878	0.911	0.906
		RMSE	0.0126	0.0111	0.0114
GC1-R	Langmuir	K_L (L/mol)	111,970	110,000	115,508
		q_e^{max} (mmol/g)	0.19	0.18	0.21
		R^2	0.985	0.827	0.936
		RMSE	0.0045	0.0157	0.0097
	Freundlich	K_F ($[10^{-3}mol^{(1-1/n)}L^{1/n}]/g$)	2150	2155	2372
		1/n	0.863	0.862	0.852
		R^2	0.913	0.887	0.960
		RMSE	0.0109	0.0128	0.0076
GC2-R	Langmuir	K_L (L/mol)	15,688	17,000	15,099
		q_e^{max} (mmol/g)	0.62	0.63	0.87
		R^2	0.914	0.917	0.981
		RMSE	0.0115	0.0108	0.0052
	Freundlich	K_F ($[10^{-3}mol^{(1-1/n)}L^{1/n}]/g$)	4032	4532	4200
		1/n	0.936	0.938	0.913
		R^2	0.906	0.905	0.978
		RMSE	0.0113	0.0115	0.0056
Chromate					
Na-R	Langmuir	K_L (L/mol)	1870	1840	1803
		q_e^{max} (mmol/g)	275	85.3	184
		R^2	0.403	0.608	0.335
		RMSE	0.2422	0.0222	0.0665
	Freundlich	K_F ($[10^{-3}mol^{(1-1/n)}L^{1/n}]/g$)	10^{20}	10^{20}	10^{17}
		1/n	3.317	3.305	2.814
		R^2	0.833	0.875	0.912
		RMSE	0.1281	0.0174	0.0246
GC1-R	Langmuir	K_L (L/mol)	1825	1886	1703
		q_e^{max} (mmol/g)	327	211	282
		R^2	0.470	0.602	0.669
		RMSE	0.2282	0.0880	0.0803
	Freundlich	K_F ($[10^{-3}mol^{(1-1/n)}L^{1/n}]/g$)	10^{21}	10^{20}	10^{21}
		1/n	3.460	3.303	3.438
		R^2	0.818	0.836	0.828
		RMSE	0.1337	0.0565	0.0579
GC2-R	Langmuir	K_L (L/mol)	1904	1882	1796
		q_e^{max} (mmol/g)	313	188	223
		R^2	0.505	0.726	0.613

(continued)

https://doi.org/10.1180/clm.2018.39 Published online by Cambridge University Press

Table 4. (*contd.*)

Adsorbent	Model	Parameters	Temperature (K)		
			298	308	318
	Freundlich	RMSE	0.2204	0.0932	0.0869
		K_F ($[10^{-3}mol^{(1-1/n)}L^{1/n}]/g$)	10^{20}	10^{20}	10^{20}
		1/n	3.305	3.321	3.304
		R^2	0.875	0.882	0.841
		RMSE	0.1109	0.0612	0.0556

MB = methylene blue.

GC2-R were not constant over the temperature range investigated.

Structural characterization and mechanisms of adsorption

Chromate adsorbents. The shape of the basal 001 reflection of stevensite was altered as a result of the interaction between chromate and the absorbents studied (Fig. 9). Taking into consideration Scherrer's formula (Ingham & Toney, 2014), the size of the crystallites of Na^+-R and GC2-R increased by ~32% and 11%, respectively, whereas no appreciable change was recorded for GC1-R.

The ^{23}Na solid-state NMR spectra of Fig. 10 indicate that the chemical environments of the exchangeable Na^+ ions ($\delta = 8.0$ ppm) and the tightly bonded ones ($\delta = -5.5$ ppm) placed within the interlayer were not disturbed by chromate adsorption.

The solid-state NMR analysis also showed that the electronic environment of the structural proton ($\delta =$ 0.4 ppm) of stevensite and that of the proton of the solvation shell ($\delta = 4.1$ ppm) of Na^+ ions were almost unaffected by chromate adsorption (Fig. 11).

Table 5. Thermodynamic data related to the adsorption processes of chromate and methylene blue (MB) onto the adsorbents studied.

Adsorbate	Adsorbent	Temperature (K)	ΔG° (kJ/mol)	Heat of adsorption (ΔH°, kJ/mol) (ΔH° = ΔG° + TΔS°)	Entropy of adsorption (ΔS°, J/K mol^{-1}) (slope of ΔG° = f(t))
MB	Na^+-R	298	−24.940	−5.570	65
		308	−25.348	−5.328	
		318	−26.236	−5.566	
	GC1-R	298	−28.790	1.308	101
		308	−29.711	1.397	
		318	−30.805	1.313	
	GC2-R	298	−23.923	−1.573	75
		308	−24.932	−1.832	
		318	−25.428	−1.578	
Chromate	Na-R	298	−10.416	12.232	76
		308	−11.283	12.125	
		318	−11.943	12.225	
	GC1-R	298	−11.300	32.208	146
		308	−12.684	32.284	
		318	−14.218	32.210	
	GC2-R	298	−11.315	–	–
		308	−12.072		
		318	−11.479		

https://doi.org/10.1180/clm.2018.39 Published online by Cambridge University Press

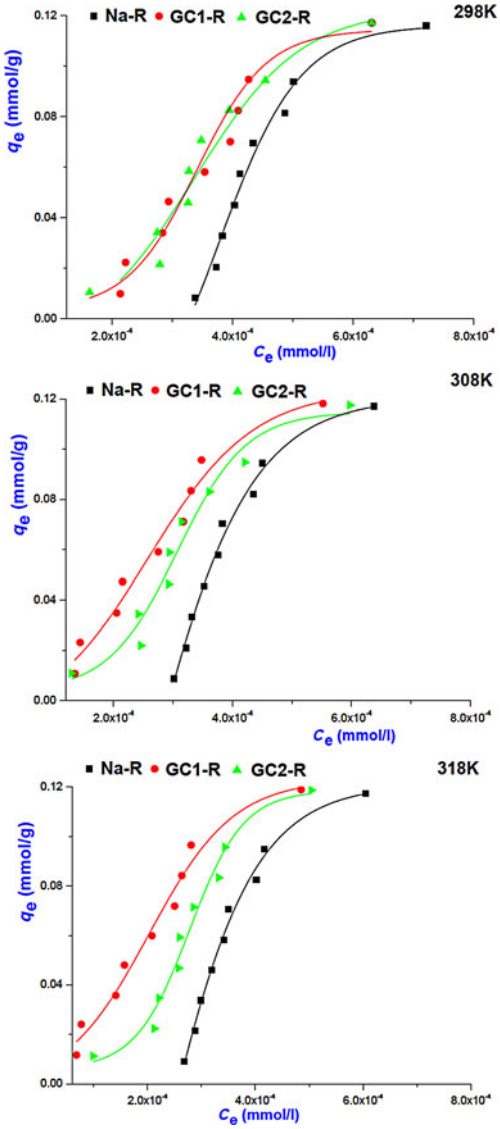

FIG. 8. Adsorption isotherms of chromate on Na^+-R and organoclays.

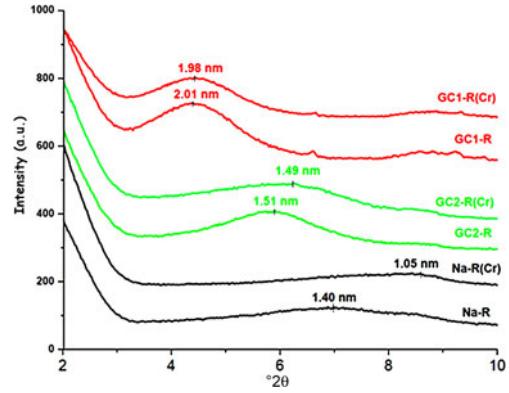

FIG. 9. X-ray diffraction patterns of the adsorbents before and after chromate retention.

Hence, the chromate was fixed to the surface and the edges of the layers of stevensite. As anionic species, hydrogen chromate (the most abundant species) seemed to develop bonds with the protonated silanols of the tetrahedral sheets (Fig. 12).

The same interaction seemed to have taken place with the protonated aluminols of the octahedral sheet. However, because the amount of Al^{IV} experienced a decrease of ~85% (Fig. 13), the $HCrO_4^-$ ions behaved differently from the protonated aluminol groups $(\equiv Al\text{-}OH_2)^+$. The Al^{3+} ions probably reacted with $HCrO_4^-$, forming complexes. In this connection, the Si^{4+} ions might not have migrated from the tetrahedral sites because of their high ionic potential (Z/R; Z and R are the charge and the radius of the cation), which was ~100 nm^{-1}.

Considering the maximum uptake amount of chromate (~0.19 mmol/g) and the specific surface area of Na^+-R (132 m^2/g), each ion was placed in an area of 1 nm^2. This represented the two basal surfaces of the unit cell of stevensite.

GC1-R was an intercalated nanocomposite. The intercalation of the dendrimers was performed by expelling all of the exchangeable Na^+ ions. On the other hand, considering the ^{27}Al NMR chemical shift before and after interaction of chromate ions with the adsorbents studied (Fig. 13), the amount of Al^{IV} of GC1-R was reduced drastically (90%) as a result of chromate adsorption, whereas that of Al^{VI} remained unchanged. The reduction in the amount of Al^{IV} was presumably due to the complexation of Al^{3+} by hydrogen chromate, as was previously mentioned. The interaction of chromate with the aluminol groups did not affect the closest environment of Si, as could be deduced from the ^{29}Si solid-state NMR spectra in Fig. 14.

The maximum quantity of chromate retained by GC1-R exceeded that of Na^+-R by ~30%. The difference was attributed essentially to the Na^+-R particle aggregation, and subsequently to the hiding of some active sites.

GC2-R consisted of exfoliated and intercalated nanocomposites, but the former structure seemed to

https://doi.org/10.1180/clm.2018.39 Published online by Cambridge University Press

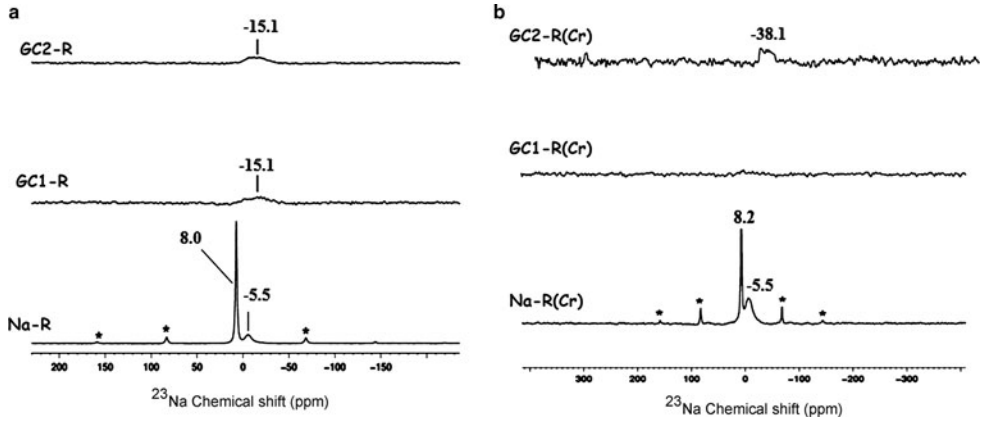

FIG. 10. ^{23}Na solid-state nuclear magnetic resonance spectra of the adsorbents. (a) Before adsorption of chromate; (b) after adsorption of chromate. *Spinning side bands.

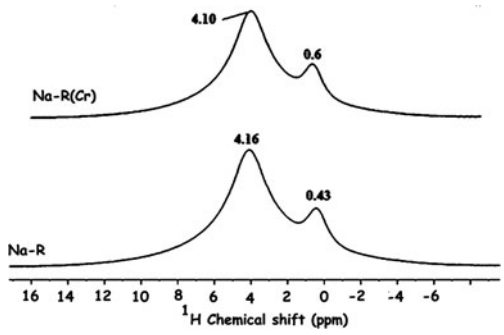

FIG. 11. ^{1}H solid-state nuclear magnetic resonance spectra of the studied adsorbents. The bands are related to the proton of the clay mineral structure (0.43, 0.6 ppm) and the proton of the solvation shell (4.16, 4.10 ppm) of Na^{+}.

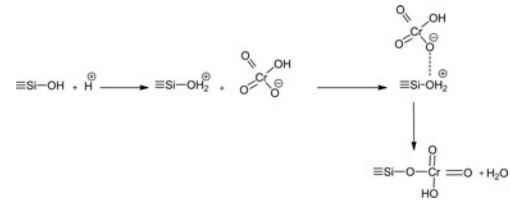

FIG. 12. Schematic representation of the interaction between hydrogen chromate and protonated silanol of the tetrahedral sheets of stevensite.

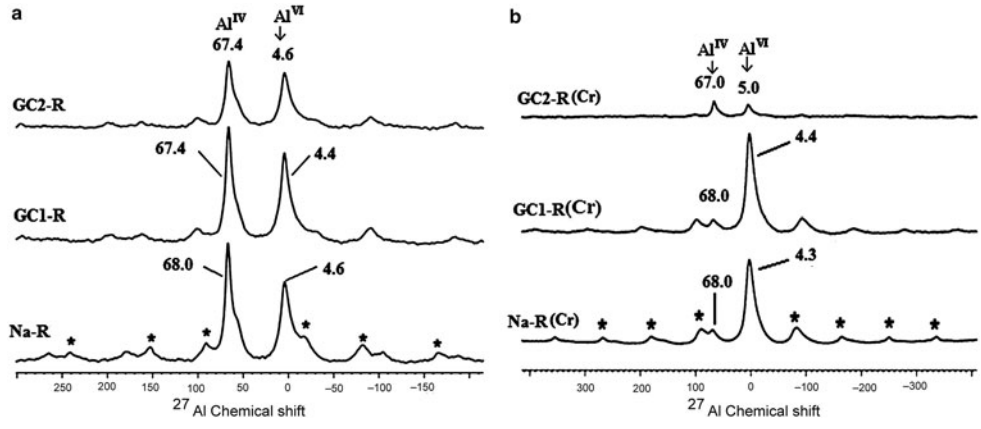

FIG. 13. ^{27}Al solid-state nuclear magnetic resonance spectra of Na^{+}-R, GC1-R and GC2-R. (a) Before adsorption of chromate; (b) after adsorption of chromate. *Spinning side bands.

https://doi.org/10.1180/clm.2018.39 Published online by Cambridge University Press

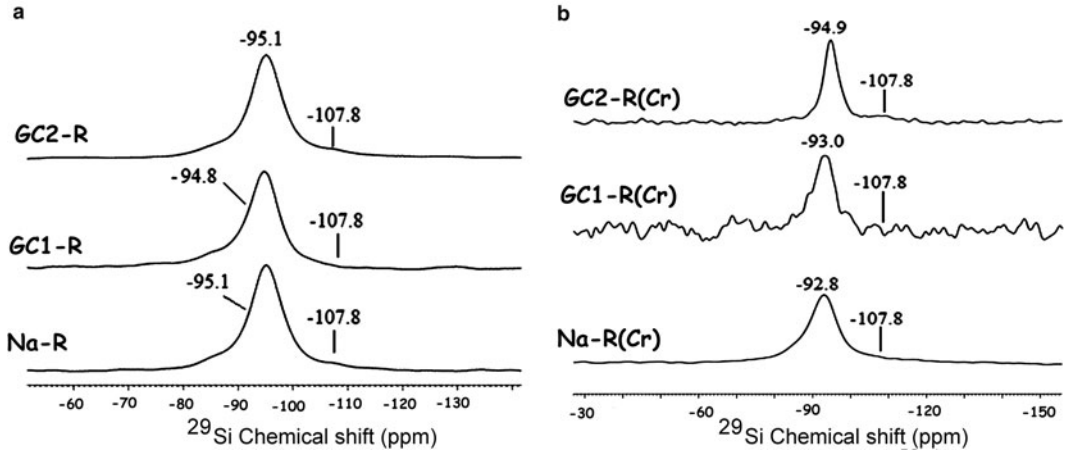

FIG. 14. ^{29}Si solid-state nuclear magnetic resonance spectra of the studied adsorbents. (a) Before contact with chromate; (b) after contact with chromate. The shoulder at –107.8 ppm is due to Si in quartz (Fernández *et al.*, 2016).

TABLE 6. Maximum uptake amounts of Cr^{VI} adsorbed by natural and modified stevensite and by the studied nanocomposites

Adsorbents	q_e^{max} (mg g^{-1})	References
Natural stevensite	0.71	Benhammou *et al.* (2007)
Al-stevensite	3.90	
Cetyltrimethylammonium bromide-stevensite	10.17	
Fe^{II}-stevensite	2.54	Benhammou *et al.* (2005)
Na^{+}-stevensite	10.53	Present study
GC1-stevensite	13.65	
GC2-stevensite	11.24	

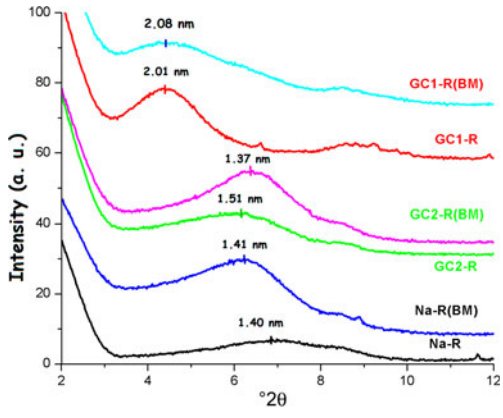

FIG. 15. X-ray diffraction traces of the adsorbents studied before and after adsorption of MB.

be predominant. Therefore, the adsorptions and the maximum amounts of chromate retained by GC2-R and Na^{+}-R were comparable.

As compared to the reported results dealing with the adsorption of chromate on modified stevensite (Table 6), the maximum uptake amount at 298 K (q_e^{max}), determined by using the linear form of the Langmuir isotherm, was slightly enhanced by dendrimer modification, particularly by GC1 intercalation. Benhammou *et al.* (2005, 2007) postulated that chromate adsorption occurred on particle edges, but they did not explain the observed differences. The chromate adsorbed mainly on the protonated aluminols and the differences between the amounts of chromate absorbed were attributed to the differences in the clay mineral particle aggregation, which was influenced by the nature of the clay mineral-modifying chemical compound.

https://doi.org/10.1180/clm.2018.39 Published online by Cambridge University Press

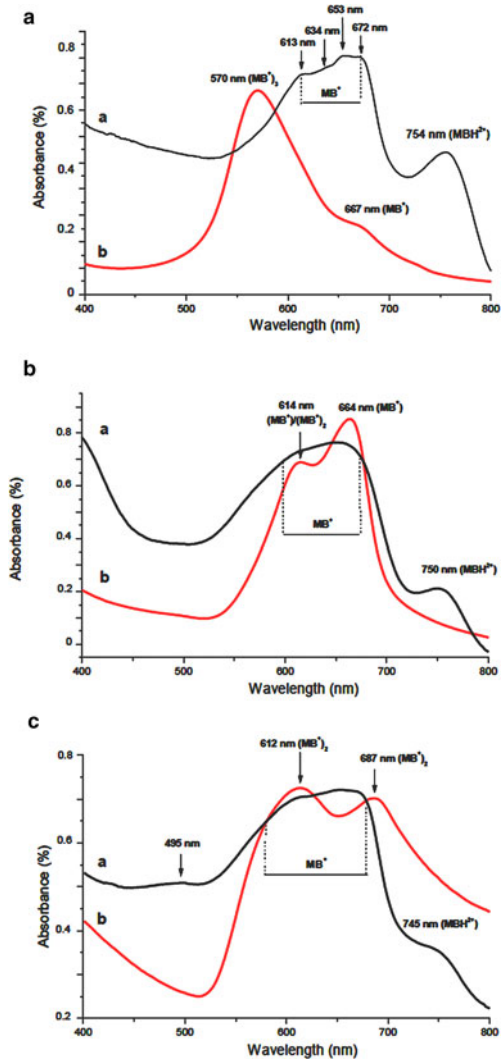

FIG. 16. UV-visible absorption spectra of the adsorbents and their corresponding supernatants after adsorption of MB. (a) Na-R; (b) GC-R; (c) GC2-R.

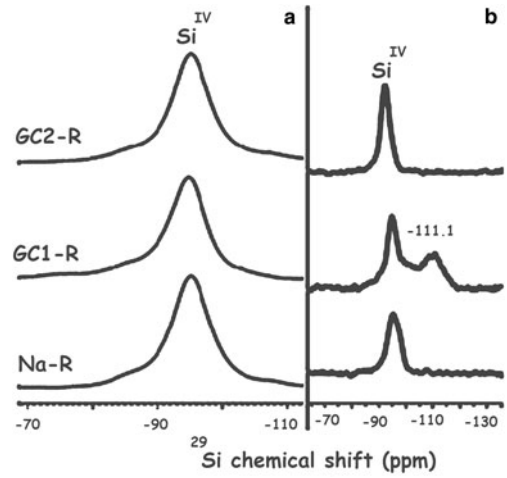

FIG. 17. ^{29}Si solid-state nuclear magnetic resonance spectra of Na^+-R, GC1-R and GC2-R. (a) Before contact with methylene blue; (b) after contact with methylene blue.

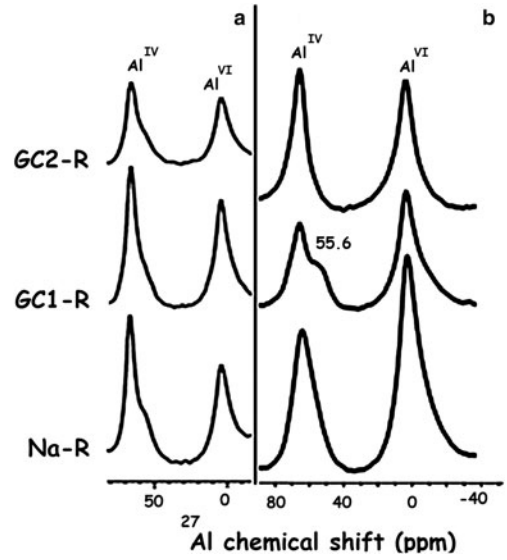

FIG. 18. ^{27}Al solid-state nuclear magnetic resonance spectra of the adsorbents. (a) Before adsorption of chromate; (b) after adsorption of chromate.

MB adsorbents. Similar to the adsorption of chromate, the shape and position of the 001 basal reflection of stevensite was modified after adsorption (Fig. 15), and the size of particles changed as a result of the adsorption of MB. The estimated increases in the size of particles were 30% and 12% for Na-R and GC2-R, respectively. For GC1-R, the size decreased by ~19%.

Considering the UV-visible spectra (Fig. 16), MB adsorbed on Na-R and on both organoclays as MBH^{2+} and MB^+. The latter species were located at the external surface of aggregates (660–675 nm) and also at the planar surface of stevensite (~653 nm). The supernatants comprised MB^+, $(MB^+)_2$ and $(MB^+)_3$, but their relative abundances varied following the adsorbent used: the trimer was abundant in the MB–Na-R contact, while the monomer and the dimer forms were formed extensively in the presence of GC1-R and GC2-R, respectively. The absence of

https://doi.org/10.1180/clm.2018.39 Published online by Cambridge University Press

MBH^{2+} in the supernatants allowed the deduction that MB protonation occurred at the surface of the particles of stevensite.

As a result of the interaction of GC1-R with MB, the structural unit Q^4 (0Al), characterized by the ^{29}Si solid NMR peak at –111.1 ppm (Fig. 17), appeared (Koller & Weiß, 2012). Moreover, the ^{29}Al solid NMR spectrum showed, in addition to the bands of Al^{VI} and Al^{IV} of stevensite, a shoulder at 55.6 ppm (Fig. 18). This was attributed to the shielded nucleus of Al^{VI}, which was probably located at the border of the structure of stevensite (He *et al.*, 2002). Such a shielding might be due to the interaction of the structural Al^{3+} at edges with MB^+ and/or MBH^{2+}. These results might be due to the aforementioned reduction in size of particles of GC1-R.

SUMMARY AND CONCLUSION

The present study yielded the following conclusions: (1) the adsorption of chromate or MB on the synthesized organoclays and Na^+ clays took place rapidly, and the kinetics followed the pseudo-second-order equation. The rate constants were in the range of 0.04–0.16 $mmol^{-1}$ g s^{-1} and 0.02–0.06 $mmol^{-1}$ g s^{-1} for chromate and MB, respectively. (2) The rates of adsorption of both chemical species were not ruled by the intraparticle diffusion or by the liquid film diffusion. (3) The adsorption isotherms of chromate correlated better with the Freundlich model, whereas those of MB were best fitted with the Langmuir model. The Gibbs free energy involved varied between –31 and –10 kJ/mol, and the adsorbent affinity for MB was relatively high ($\Delta G°$[MB] ≈ $2\Delta G°$[chromate]). (4) The maximum uptake amounts of MB and Cr^{VI} were in the ranges of 0.15–0.90 mmol/g and 10–14 mg/g, respectively. GC2-R and GC1-R were the best adsorbents for MB and chromate, respectively. (5) Chromate ions, which were present extensively as $HCrO_4^-$, were fixed to the protonated silanols and aluminols of the edges and the free surfaces of the stevensite layers. (6) Due to the adsorption of chromate, most of the tetrahedral aluminium was removed from the structure of stevensite, and probably formed complexes with chromate ions. (7) MB was retained as MB^+ and MBH^{2+}. The cations of the former species were placed at the planar surfaces of stevensite and the external surfaces of aggregates. The latter species formed at the clay surfaces. (8) As a result of MB adsorption on GC1-R, the structural unit Q^4(0Al) was formed. In this case, Al^{VI} at the edges of the stevensite layers seemed to be abundant and contributed to the adsorption of MB.

ACKNOWLEDGMENTS

The authors are grateful to CNRS (France), CNRST (Morocco), Campus-France (France) and the LIA LCMMF for their financial support.

REFERENCES

Ajouyed O., Hurel C., Ammari M., BenAllal L. & Marmier N. (2010) Sorption of Cr(VI) onto natural iron and aluminum (oxy)hydroxides: effects of pH, ionic strength and initial concentration. *Journal of Hazardous Materials*, **174**, 616–622.

Akar S.T., Yetimoglu Y. & Gedikbey T. (2009) Removal of chromium (VI) ions from aqueous solutions by using Turkish montmorillonite clay: effect of activation and modification. *Desalination*, **244**, 97–108.

Al Othman Z. A. (2012) A review: fundamental aspects of silicate mesoporous materials. *Materials*, **5**, 2874–2902.

Aran D., Maul A. & Masfaraud J.F. (2008) A spectrophotometric measurement of soil cation exchange capacity based on cobaltihexamine chloride absorbance. *Comptes Rendus Geoscience*, **340**, 865–871.

Benhammou A., Yaacoubi A., Nibou L. & Tanouti B. (2005) Study of the removal of mercury(II) and chromium(VI) from aqueous solutions by Moroccan stevensite. *Journal of Hazardous Materials*, **117**, 243–249.

Benhammou A., Yaacoubi A., Nibou L. & Tanouti B. (2007) Chromium (VI) adsorption from aqueous solution onto Moroccan Al-pillared and cationic surfactant stevensite. *Journal of Hazardous Materials*, **140**, 104–109.

Beraa A., Hajjaji M., Laurent R., Delavaux-Nicot B. & Caminade A.-M. (2016) Removal of chromate from aqueous solutions by dendrimers–clay nanocomposites. *Desalination and Water Treatment*, **57**, 14290–14303.

Beraa A., Hajjaji M., Laurent R., Delavaux-Nicot B. & Caminade A.-M. (2017) Dendrimers-containing organoclays: characterisation and interaction with methylene blue. *Applied Clay Sciences*, **136**, 142–151.

Bouna L., Rhouta B., Amjoud M., Jada A., Maury F., Daoudi L. & Senocq F. (2010) Correlation between eletrokinetic mobility and ionic dyes adsorption of Moroccan stevensite. *Applied Clay Science*, **48**, 527–530.

Caminade A.M. & Majoral J.P. (2016) Bifunctional phosphorus dendrimers and their properties. *Molecules*, **21**, 538.

Chakraborty U., Singha T., Chianelli R.R., Hansda C. & Paul K.P. (2017) Organic–inorganic hybrid layer-by-

https://doi.org/10.1180/clm.2018.39 Published online by Cambridge University Press

layer electrostatic self-assembled film of cationic dye methylene blue and a clay mineral: spectroscopic and atomic force microscopic investigations. *Journal of Luminescence*, **187**, 322–332.

Chang J., Ma J., Ma Q., Zhang D., Qiao N., Hu M. & Ma H. (2016) Adsorption of methylene blue onto Fe_3O_4 activated montmorillonite nanocomposite. *Applied Clay Sciences*, **119**, 132–140.

Christidis G.E. & Koutsopoulou E. (2013) A simple approach to the identification of trioctahedral smectites by X-ray diffraction. *Clay Minerals*, **48**, 687–696.

Cottet L., Almeida C.A.P., Naidek N., Viante M.F., Lopes M.C. & Debacher N.A. (2014) Adsorption characteristics of montmorillonite clay modified with iron oxide with respect to methylene blue in aqueous media. *Applied Clay Science*, **95**, 25–31.

Degen T., Sadki M., Bron E., König U. & Nénert G. (2014). The HighScore suite. *Powder Diffraction* **29** (Supplement S2), S13–S18.

Elass K., Laachach A., Alaoui A. & Azzi M. (2011) Removal of methyl violet from aqueous solution using a stevensite-rich clay from Morocco. *Applied Clay Science*, **54**, 90–96.

Fernández R., Ruiz A.I. & Cuevas J. (2016) Formation of C-A-S-H phases from the interaction between concrete or cement and bentonite. *Clay Minerals*, **51**, 223–235.

Freundlich H. (1907) Über die adsorption in Lösungen. *Zeitschrift für Physikalische Chemie.*, **57**, 385–470.

Fu F. & Wang Q. (2011) Removal of heavy metal ions from wastewaters: a review. *Journal of Environmental Management*, **92**, 407–418.

Hajjaji M. & Beraa A. (2015) Chromate adsorption on acid-treated and amines-modified clay. *Applied Water Science*, **5**, 73–79.

Hameau A., Fruchon S., Bijani C., Badrucci A., Blanzat M., Poupot R., Pavan G.M., Caminade A.M. & Turin C.O. (2015) Theoretical and experimental characterization of amino-PEG-phosphonate-terminated polyphosphorhydrazone dendrimers: influence of size and PEG capping on cytotoxicity profiles. *Journal of Polymer Science Part A: Polymer Chemistry*, **53**, 761–774.

Harkins W.D. & Jura G. (1943) An adsorption method for the determination of the area of a solid without the assumption of a molecular area, and the area occupied by nitrogen molecules on the surfaces of solids. *Journal of Chemical Physics*, **11**, 431–432.

He H., Guo J., Xie X., Lin H. & Li L. (2002) A microstructural study of acid-activated montmorillonite from Choushan, China. *Clay Minerals*, **37**, 337–344.

Heinz H. (2012) Clay minerals for nanocomposites and biotechnology: surface modification, dynamics and responses to stimuli. *Clay Minerals*, **47**, 205–230.

Hossain M.A., Ngo H.H. & Guo W. (2013) Introductory of Microsoft Excel Solver function-Spreadsheet method for isotherm and kinetics modeling of metals biosorption in water and wastewater. *Journal of Water Sustainabililty*, **3**, 223–237.

Ingham B. & Toney M.F. (2014) X-ray diffraction for characterizing metallic films. Pp. 3–8 in: *Metallic Films for Electronic, Optical and Magnetic Applications. Structure, Processing and Properties* (K. Barmak & K. Coffey, editors). Woodhead Publishing – Elsevier, Cambridge, UK.

Ismadji S., Edi Soetaredjo F. & Aning Ayucitra A. (2015) *Clay Materials for Environmental Remediation*. Springer, New York, NY, USA.

Koller H. & Weiß M. (2012) Solid state NMR of porous materials. Pp. 189–227 in: *Solid State NMR* (J.C.C. Chan, editor). Springer-Verlag GmbH, Berlin, Germany.

Krupskaya V.V., Zakusin S.V., Tyupina E.A., Dorzhieva O.V., Zhukhlistov A.P., Belousov P.E. & Timofeeva M.N. (2017) Experimental study of montmorillonite structure and transformation of its properties under treatment with inorganic acid solutions. *Minerals*, **7**, 49.

Langmuir I. (1918) The adsorption of gases on plane surfaces of glass, mica and platinum. *Journal of the American Chemical Society*, **40**, 1361–1403.

Lee S.M. & Tiwari D. (2012) Organo and inorgano–organo-modified clays in the remediation of aqueous solutions: an overview. *Applied Clay Science*, **59–60**, 84–102.

Mache J.R., Signing P., Mbey J.A., Razafitianamaharavo A., Njopwouo D. & Fagel N. (2015) Mineralogical and physico-chemical characteristics of Cameroonian smectitic clays after treatment with weakly sulfuric acid. *Clay Minerals*, **50**, 649–661.

Mailer A.G., Clegg P.S. & Pusey P.N. (2015) Particle sizing by dynamic light scattering: non-linear cumulant analysis. *Journal of Physics: Condensed Matter*, **27**, 145102.

Padié C., Maszewska M., Majchrzak K., Nawrot B., Caminade A.M. & Majoral J.P. (2009) Polycationic phosphorus dendrimers: synthesis, characterization, study of cytotoxicity, complexation of DNA, and transfection experiments. *New Journal of Chemistry*, **33**, 318–326.

Qiu H., Lv L., Pan B.-C., Zhang Q.-J., Zhang W.-M. & Zhang Q.-X. (2009) Critical review in adsorption kinetic models. *Journal of Zhejiang University – SCIENCE A*, **10**, 716–724.

Ranđelović M.S., Purenović M.M., Matović B.Z., Zarubica A.R., Momčilović M.Z. & Purenović J.M. (2014) Structural, textural and adsorption characteristics of bentonite-based composite. *Microporous and Mesoporous Materials*, **195**, 67–74.

Rathnayake S.I., Martens W.N., Xi Y., Frost R.L. & Ayoko G.A. (2017) Remediation of Cr(VI) by

https://doi.org/10.1180/clm.2018.39 Published online by Cambridge University Press

inorganic–organic clay. *Journal of Colloid and Interface Science*, **490**, 163–173.

Ren X., Zhang Z., Luoa H., Huc B., Dang Z., Yanga C. & Li L. (2014) Adsorption of arsenic on modified montmorillonite. *Applied Clay Science*, **97–98**, 17–23.

Saha R., Nandi R. & Saha B. (2011) Sources and toxicity of hexavalent chromium. *Journal of Coordination Chemistry*, **64**, 1782–1806.

Santhana A., Kumar K., Ramachandran R., Kalidhasan S., Rajesh V. & Rajesh N. (2012) Potential application of dodecylamine modified sodium montmorillonite as an effective adsorbent for hexavalent chromium. *Chemical Engineering Journal*, **211–212**, 396–405.

Sarkar B., Xi Y., Megharaj M., Krishnamurti G.S.R., Rajarathnam D. & Naidu R. (2010) Remediation of hexavalent chromium through adsorption by bentonite based Arquad® 2HT-75 organoclays. *Journal of Hazardous Materials*, **183**, 87–97.

Setshedi K.Z., Bhaumik M., Songwane S., Onyango M.S. & Maity A. (2013) Exfoliated polypyrrole-organically modified montmorillonite clay nanocomposite as a potential adsorbent for Cr(VI) removal. *Chemical Engineering Journal*, **222**, 186–197.

Shokri E., Yegani R. & Akbarzadeh A. (2017) Novel adsorptive mixed matrix membranes by embedding modified montmorillonite with arginine amino acid into polysulfones for As(V) removal. *Applied Clay Science*, **144**, 141–149.

Soares R., Carneiro M.C., Monteiro M.I.C., Henrique S. S., Jr, Pontes F.V.M., Silva L.D., Neto A.A. & Santelli R.E. (2009) Simultaneous speciation of chromium by spectrophotometry and multicomponent analysis. *Chemical Speciation and Bioavailability*, **21**, 153–160.

WHO (2003) *Chromium in Drinking-Water. Background Document for Preparation of WHO Guidelines for Drinking-Water Quality*. World Health Organization, Geneva, Austria.

Zhao Y., Yang S., Ding D., Chen J., Yang Y., Lei Z., Feng C. & Zhang Z. (2013) Effective adsorption of Cr (VI) from aqueous solution using natural Akadama clay. *Journal Colloid and Interface Science*, **395**, 198–204.

Zhitkovich A. (2011) Chromium in drinking water: sources, metabolism, and cancer risks. *Chemical Research in Toxicology*, **24**, 1617–1629.

https://doi.org/10.1180/clm.2018.39 Published online by Cambridge University Press